Decay of ^{147}Tm and the role of triaxiality studied with a nonadiabatic quasiparticle approach

Swati Modi, M. Patial,* and P. Arumugam†
Department of Physics, Indian Institute of Technology Roorkee, Roorkee 247667, India

L. S. Ferreira
Centro de Física e Engenharia de Materiais Avançados CeFEMA, and Departmento de Física, Instituto Superior Técnico, Universidade de Lisboa, Avenida Rovisco Pais, P1049-001 Lisbon, Portugal

E. Maglione
Dipartimento di Fisica e Astronomia "G. Galilei", and Istituto Nazionale di Fisica Nucleare, Via Marzolo 8, I-35131 Padova, Italy
(Received 12 September 2017; published 6 December 2017)

We study the structure and decay properties of triaxially deformed odd-A proton emitter ^{147,147m}Tm with the modified particle-rotor model, which utilizes the microscopic nonadiabatic quasiparticle approach. In this approach the core spectrum is coupled with the particle states and hence the rotor properties are carried forward to the odd-A system. We demonstrate the merits of this approach by explaining the measured rotational bands in the triaxial proton emitters ^{141}Ho and ^{145,147}Tm. With our calculated spectra and half-lives for the proton emission, we confirm the ground state of ^{147}Tm to be $11/2^-$ and predict the positive parity isomeric state to be $5/2^+$.

DOI: 10.1103/PhysRevC.96.064308

I. INTRODUCTION

The drip line nuclei attract extensive interest due to continuous development of radioactive ion beam facilities yielding data yet to be understood [1]. These nuclei around the proton drip line exhibit unique phenomena such as spontaneous proton emission. The proton emission from the ground state was first observed in ^{151}Lu [2] followed by ^{147}Tm [3] with the online mass separator at GSI (Darmstadt). Later, many other nuclei with $51 \leqslant Z \leqslant 83$ were identified as ground state proton emitters [4]. The study of proton emitters enables us to isolate the specific aspect of nuclear interaction due to the excess of protons, which is important for both nuclear physics and astrophysics. In astrophysics the rapid-proton capture process (rp process), which is inverse of the proton emission, helps to map the proton drip line. The analysis of proton emission half-life, branching ratio, energy, and the orbital angular momentum carried away by the emitted proton provide a stringent test for theoretical models aimed at a unified description of all these quantities.

The proton emission has been studied extensively for spherical and deformed nuclei in past decades [5]. Decays of proton emitters are easily described by models based on semiclassical Wentzel-Kramers-Brillouin methods [6–8]. More detailed information, including the structure aspects, are obtained from microscopic studies of deformed nuclei by considering proton emission from the single-particle Nilsson level arising from the resonance of the particle-core unbound system in the adiabatic limit [9–11]. The nonadiabatic quasiparticle approach is quite successful in unveiling the structure and decay properties of the axially [12–15] and triaxially deformed proton emitters [16–18]. In the nonadiabatic quasiparticle approach either a constant moment of inertia (rigid rotor) or a variable moment of inertia (VMI) is utilized in the rotation-particle coupling through a particle-rotor model (PRM). The VMI looks reasonable since the nucleus possesses nonrigidity. If the core energies are directly employed in the rotation-particle coupling procedure then there is no need to assume any moment of inertia. Such an approach is used to describe the axially deformed proton emitters [19,20] and, in the adiabatic limit, the triaxially deformed proton emitters [21]. In this work we are using a microscopic nonadiabatic approach for rotation-particle coupling in triaxial nuclei, which we termed the modified particle-rotor model (MPRM) [22]. In this approach the experimental core energies are employed to couple with the particle states and describe the interesting features of nuclei such as strong triaxial deformation γ and its effect on rotation alignment plot, and the rotational spectra including ground and side bands. We have extended this approach to study the rotational states of proton emitters, and the MPRM wave functions are utilized to calculate the decay widths of proton emitters in a fully microscopic way [23].

In the present work we discuss the outline of our formalism and its application to ^{141}Ho, ^{145}Tm, and ^{147}Tm. Both the ground and isomeric states of ^{141}Ho are proton emitting states with 100% proton emission branch. The isotopes ^{145}Tm and ^{147}Tm are also investigated to bring out their inherent properties. The ground and isomeric states of ^{147}Tm are proton emitting states as in ^{141}Ho, but with proton emission branches of 15(5)% and 100%, respectively [24,25]. The rest of the ground state [85(5)%] decays through β^+ and electron capture [26]. The microscopic calculations for finding the decay properties of ^{147}Tm are performed for the first time with our MPRM.

II. THEORETICAL FRAMEWORK

The Hamiltonian for an odd-A nucleus is given by the sum of the triaxially deformed mean field of single particles $H_{\rm av}$,

*Present address: Department of Physics, Worcester Polytechnic Institute, Worcester, MA 01609.
†p.arumugam@gmail.com

the pairing interaction $H_{\rm pair}$, and the Hamiltonian for the rotor (core) $H_{\rm rot}$. Thus

$$H = H_{\rm av} + H_{\rm pair} + H_{\rm rot}. \tag{1}$$

The wave function of an odd-A system can be written as

$$\Psi_{IM}(\vec{r},\omega) = \sum_{ljR\tau} \frac{\phi^I_{ljR\tau}(r)}{r} |ljR\tau, IM\rangle, \tag{2}$$

where $\vec{r}$ is the position of the proton and ω is the orientation of the core in the laboratory frame. $\phi^I_{ljR\tau}(r)/r$ and $|ljR\tau, IM\rangle$ are the radial and angular parts of the wave function, respectively. The orbital and the total angular momenta of the particle are given by l and j, respectively. I is the total angular momentum of the odd-A system with its projections M and K on the z axis (laboratory frame) and the third axis (body fixed frame), respectively. Similarly, we have the total angular momentum of rotor R and its projections τ and K_R.

The quantum numbers R and K_R are utilized to form the basis for the rotor Hamiltonian $H_{\rm rot}$. The transformation between the R and K representations is obtained with the transformation amplitude

$$A^{IK}_{j\Omega_p,RK_R} = \sqrt{\frac{2R+1}{2I+1}} \langle j\Omega_p RK_R | IK\rangle \sqrt{1+\delta_{K_R,0}}, \tag{3}$$

where Ω_p is the projection of j on the third axis. With the help of above transformation amplitude, the rotor's energies E_{TRi}, and eigenvectors $c^{Ri}_{K_R}$, the matrix elements of $H_{\rm rot}$ in the K representation [22,23,27] can be written as

$$\begin{aligned}
&\langle lj\Omega_{p'}K', IM|H_{\rm rot}|lj\Omega_pK, IM\rangle \\
&= \sum_{R,K_{R'},K_R} A^{IK'}_{j\Omega_{p'},RK_{R'}} \sum_i c^{Ri}_{K_{R'}} E_{TRi} c^{Ri}_{K_R} A^{IK}_{j\Omega_p,RK_R} \\
&= W^{K'K}_{j\Omega_{p'}\Omega_p}.
\end{aligned} \tag{4}$$

Here, the matrix element $W^{K'K}_{j\Omega_{p'}\Omega_p}$ is termed the coupling matrix. i labels the different eigenstates for a given value of R. The matrix elements of the particle-plus-rotor system can be written in the K representation as

$$\begin{aligned}
&\langle q'K', IM|H|qK, IM\rangle \\
&= \epsilon_q\, \delta_{K'K}\delta_{q'q} + \sum_{lj\Omega_{p'}\Omega_p} W^{K'K}_{j\Omega_{p'}\Omega_p} \\
&\quad \times \int dr\, f_{uv}\, \phi^{IK'*}_{lj\Omega_{p'}}(r)\, \phi^{IK}_{lj\Omega_p}(r).
\end{aligned} \tag{5}$$

Here, q defines the single-particle state. ϵ_q is the quasiparticle energy, which is calculated from the single-particle energy (e_q) through the relation $\epsilon_q = \sqrt{\Delta^2 + (e_q-\lambda)^2}$. The single-particle energies e_q and wave functions $\phi^{IK}_{lj\Omega_p}(r)$ are calculated by $H_{\rm av}$, which consists of the triaxially deformed Woods-Saxon potential along with the Coulomb and the spin-orbit interactions. We consider the pairing interaction through the BCS approach with a frozen gap $\Delta = 12/\sqrt{A}$ MeV [28]. The chemical potential λ is calculated by imposing particle number conservation. In the BCS approach, the occupation (V_q) and unoccupation (U_q) probabilities are given by the relations $V_q^2 = \frac{1}{2}[1-(e_q-\lambda)/\epsilon_q]$ and $V_q^2 + U_q^2 = 1$. The factor $f_{uv} = (U_qU_{q'} + V_qV_{q'})$ is utilized to transform the matrix element from the particle states to the quasiparticle states.

In Eq. (4), the experimental rotor energies are utilized as E_{TRi}. For the unavailable data and the rotor eigenvectors $c^{Ri}_{K_R}$, the variable moment of inertia (VMI) approach is used (VMI method 2 of Ref. [22]), which is formulated in the following text.

Hamiltonian for the triaxial rigid rotor (core) is given by

$$H_{\rm rot} = \sum_{k=1,2,3} \frac{\hbar^2 R_k^2}{2\mathcal{I}_k}, \tag{6}$$

where $\mathcal{I}_k$ are the moments of inertia. The rotor energies E_{Ri} can be calculated through the relation

$$H_{\rm rot}|RM_Ri\rangle = E_{Ri}|RM_Ri\rangle. \tag{7}$$

The eigenfunction [29] can be written is terms of the basis wave functions as

$$|RM_Ri\rangle = \sum_{K_R} c^{Ri}_{K_R} |RM_RK_R\rangle, \tag{8}$$

where i labels the different eigenstates for a given value of R, with $c^{Ri}_{K_R}$ specifying the contribution of each K_R. M_R is the projection of R on the z axis. The even-even rotor may not be a rigid rotor. The nonrigidity can be employed by VMI. We write the total energy E_{TRi} as the sum of the potential energy and the rotational energy [30,31] of the core. Thus the total energy

$$E_{TRi} = \frac{1}{2}C(\mathcal{I}_{0Ri} - \mathcal{I}_0)^2 + \frac{1}{2\mathcal{I}_{0Ri}}\eta_{Ri}\,, \tag{9}$$

where C and $\mathcal{I}_0$ are the VMI parameters. These parameters correspond to the measure of softness in the nucleus. The softness parameter is given by $\sigma = \frac{1}{C\mathcal{I}_o^3}$ [30]. The moments of inertia are in units of $\hbar^2$. The quantity $\eta_{Ri} = 2\mathcal{I}_{0Ri}E_{Ri}$ is dimensionless. For calculating E_{Ri}, the moment of inertia $\mathcal{I}_{kRi}$ is needed, which is related to $\mathcal{I}_{0Ri}$ and the triaxial deformation parameter γ through the hydrodynamical relation

$$\mathcal{I}_{kRi} = \frac{4}{3}\mathcal{I}_{0Ri}\sin^2\left(\gamma - \frac{2\pi k}{3}\right). \tag{10}$$

$\mathcal{I}_{0Ri}$ is the moment of inertia at $\gamma = 0$. The VMI parameters C and $\mathcal{I}_0$ along with the triaxial deformation γ are obtained through the equilibrium condition $\partial E_{TRi}/\partial\mathcal{I}_{0Ri} = 0$ and the error minimization of E_{TRi} with the experimental core energies [22].

The influence of γ deformation in a rotor spectrum can be manifested by a simpler method. The variable moment of inertia $\mathcal{I}_k$ is given by

$$\mathcal{I}_k = \mathcal{I}_0(R)\,\sin^2\left(\gamma - \frac{2\pi k}{3}\right),$$

where

$$\mathcal{I}_0(R) = \mathcal{I}_0\sqrt{1+bR(R+1)}, \tag{11}$$

with the VMI parameter b [32]. $\mathcal{I}_0$ is calculated with the expression $\frac{1}{2\mathcal{I}_0\sqrt{1+6b}} = \frac{E_{2^+}}{6}$ [33]. We label this method as VMI-1 and the previously outlined method as VMI-2.

The decay width is obtained from the overlap of initial (parent) and final state wave functions. The final state wave

function is given by the coupling of the daughter and the outgoing proton wave functions [12]. The partial decay width for the triaxial odd-A nucleus is given by

$$\Gamma_{lj}^{IR} = \frac{2(2R+1)}{2I+1}\frac{\hbar^2\kappa}{\mu}\left|\sum_{qK,\Omega}{}' \sum_{K_R} g^{\tau}_{RK_R}\langle RK_R j\Omega|IK\rangle\, a^I_{q,K}\, U^f_q \times \frac{\phi^{q\Omega}_{lj}(r)}{G_l(\kappa r)+iF_l(\kappa r)}\right|^2. \quad (12)$$

Here, F and G are the regular and irregular Coulomb wave functions, respectively. $\phi^{q\Omega}_{lj}(r)$ are the radial wave functions of the outgoing proton carrying a wave vector κ. μ is the reduced mass of the core-proton system. The quantities $a^I_{q,K}$ are the mixing coefficients for the parent nucleus. $|U^f_q|^2$ is the probability that the proton single-particle state in the daughter nucleus is empty. For proton decay to the ground state of the daughter nucleus, $g^{\tau}_{0,0} = 1$, and for decay to the lowest 2^+ state ($\tau = 1$),

$$g^1_{2,K_R} = \frac{1}{\sqrt{1+|K_R|/2}}\left[\frac{1}{2} + (-1)^{K_R/2}\mathcal{F}(\gamma)\right], \quad (13)$$

where

$$\mathcal{F}(\gamma) = \frac{\sin\gamma\sin 3\gamma + 3\cos\gamma\cos 3\gamma}{2(9-8\sin^2 3\gamma)^{1/2}}. \quad (14)$$

If the proton is decaying to the ground state of the daughter nucleus ($R = 0$), the angular momentum of the escaping proton (j) will be equal to the angular momentum of the parent nucleus (I). If decay happens to the excited state ($R \neq 0$) of the daughter nucleus, the emitted proton can take a range of angular momenta $|I - R| \leqslant j \leqslant I + R$. The total decay width is obtained by

$$\Gamma^{IR} = \sum_{j=|R-I|}^{j=R+I} \Gamma^{IR}_{lj}. \quad (15)$$

The branching ratio between the decay to the ground and first excited 2^+ states is obtained through $\Gamma^{I2}/(\Gamma^{I2}+\Gamma^{I0})$. The half-life is obtained using the expression $T_{1/2} = \hbar\ln 2/\Gamma$.

III. RESULTS AND DISCUSSIONS

We start our analysis with the application of our new formalism to the proton emitters whose triaxiality is well established. A nonadiabatic quasiparticle approach comprising a simple PRM (with VMI-1) has been applied to ascertain the role of triaxiality in the structure and decay of ^{141}Ho [16] and ^{145}Tm [17]. As a first step, we study the consequence of replacing PRM with MPRM for these nuclei. This effect is pronounced only in the rotational spectra, as discussed in the forthcoming text.

The ground state of ^{141}Ho is the proton emitting state with the decay leading to the daughter nucleus ^{140}Dy. In Fig. 1, we present the rotational spectrum of ^{140}Dy built on its ground state, calculated with the methods VMI-1 and VMI-2. Both the VMI methods provide a good correspondence with the experimental data at $\gamma = 20^\circ$. The results of VMI-1 provide clear evidence of triaxiality in ^{140}Dy [16]. VMI-2 yields a good agreement with data but the results are not sensitive to the asymmetry parameter γ. The data of the γ band are more crucial for evaluating γ [31]. The parameters C and $\mathcal{I}_0$ for ^{140}Dy in Fig. 1 correspond to a smaller value of the softness parameter σ. Similarly, the small value of b indicates stiffness. These values suggest that ^{140}Dy is a rigid rotor with a very small vibration-like component.

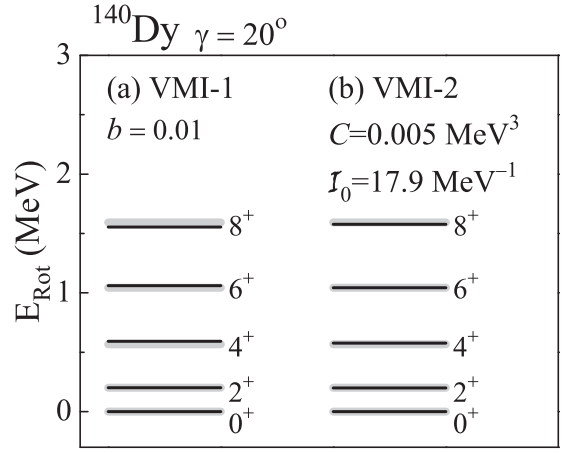

FIG. 1. Ground state rotational spectrum of ^{140}Dy with (a) the parameter b dependent VMI-1 [16] and (b) parameters C and $\mathcal{I}_0$ dependent VMI-2 for the triaxial rotor. The spectrum is presented at $\gamma = 20^\circ$ obtained through the best fitting of the data. Grey lines correspond to the experimental spectrum [34,35] and are used in the fit.

The positive parity rotational spectrum of a particle-plus-core system (^{141}Ho) with the PRM [16] and MPRM is presented in Fig. 2. The deformation parameters $\beta_2 = 0.24$ and $\beta_4 = -0.046$ are chosen to be consistent with Ref. [16]. Both the methods suggest $\gamma \sim 20^\circ$ for ^{141}Ho. With the PRM, the low lying angular momentum states do not have good correspondence with the data, but higher lying levels are comparatively better reproduced. The results of MPRM for

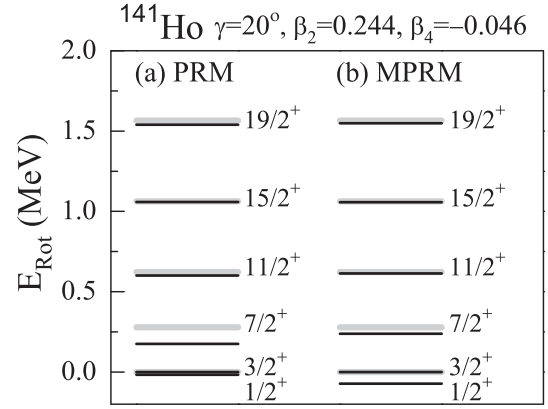

FIG. 2. Excited state positive parity spectrum of ^{141}Ho at $\gamma = 20^\circ$, $\beta_2 = 0.244$, and $\beta_4 = -0.046$. Grey lines correspond to the experimental spectrum [36]. The black lines represent the results of (a) the particle rotor model (PRM) [16] and (b) our calculation with MPRM.

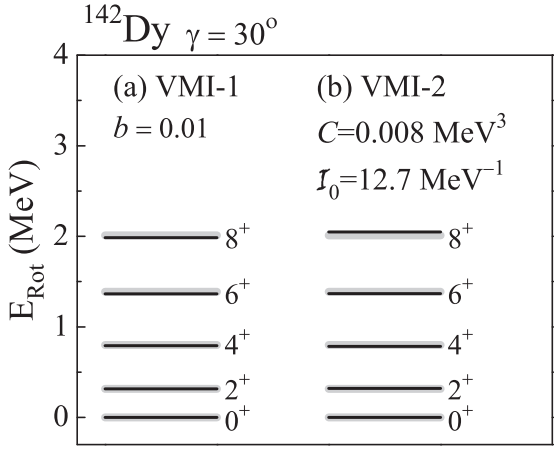

FIG. 3. Similar to Fig. 1 but for ^{142}Dy at $\gamma = 30^{\circ}$. Grey lines correspond to the experimental spectrum [37] and are used in the fit.

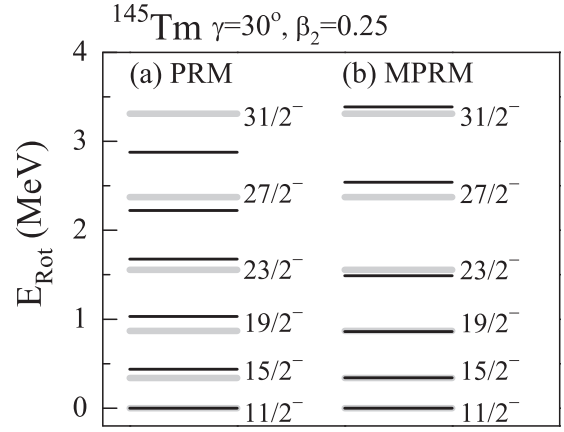

FIG. 4. Similar to Fig. 2 but for the ground state spectrum of ^{145}Tm at $\gamma = 30^{\circ}$ and $\beta_2 = 0.25$. Grey lines correspond to the experimental spectrum [38].

the whole positive parity band give excellent agreement with the experimental data. Thus one can observe that the rotational spectrum of ^{141}Ho is better reproduced by the MPRM than the PRM. The decay width and branching ratios of proton emission from both the ground and isomeric states of ^{141}Ho calculated with MPRM are consistent with the results of PRM [16] and are not shown here.

Similar inferences can be derived from the investigation of the rotational spectrum of the ground state proton emitter ^{145}Tm. The experimental data of the ground state spectrum of the core ^{144}Er are not available yet and hence the spectrum of ^{142}Dy is considered. In our theory we assume that the valence proton moves in the mean field generated by the core. This implies that the deformations of the parent and core nuclei should be same. The deformation of ^{142}Dy ($\beta_2 = 0.219$, $\beta_4 = -0.049$) is comparable with that of ^{145}Tm ($\beta_2 = 0.249$, $\beta_4 = -0.078$) as predicted by the macroscopic-microscopic calculations [39]. In Fig. 3, we present the spectrum of ^{142}Dy calculated with the methods VMI-1 and VMI-2. Here also the data for the ground band only are available and both the VMI approaches yield good agreement with data. Similar to ^{140}Dy, the VMI parameters b of VMI-1 and C and $\mathcal{I}_0$ of VMI-2 show that the core ^{142}Dy behaves like a rigid rotor with a very small vibration-like component. The ground state spectrum of ^{145}Tm calculated with PRM and MPRM are presented in Fig. 4 along with the measured data. The chosen β_2 is consistent with Ref. [17]. Both the methods suggest the triaxial deformation $\gamma = 30^{\circ}$ for ^{145}Tm. Here also, the results from MPRM have better agreement with the data when compared to PRM. The decay width and branching ratio of proton emission from ^{145}Tm calculated with MPRM (not shown here) are similar to those presented in Ref. [17]. From the results of ^{141}Ho and ^{145}Tm, it is clear that the MPRM, which has minimal set of adjustable parameters, could provide more accurate description of the rotational spectrum, whereas the accuracy of PRM is sufficient to explain the proton emission data. With the use of MPRM, the unified description of rotational spectra and decay width of proton emitters emerges to be unambiguous. Application of this approach to the proton emitter ^{147}Tm is discussed below.

The core of ^{147}Tm is ^{146}Er, for which experimental data are not available. We consider the next nearest neighbor ^{144}Dy as a core. ^{147}Tm is predicted to be triaxially deformed with $\beta_2 = 0.21$ and $\gamma = 28.16^{\circ}$ through triaxial RMF+BCS calculations [40], and its core ^{144}Dy is also predicted to be triaxially deformed with $\beta_2 = 0.20$ and $\gamma = 25^{\circ}$ from macroscopic-microscopic calculations [41]. In Fig. 5, we present the VMI-1 results for ^{144}Dy, which clearly demonstrate triaxiality in ^{144}Dy with $\gamma \sim 25^{\circ}$. At zero γ, the calculated spectrum is far from the observed one and, even with a very large value of b, one can not reproduce the data. We present in Fig. 6 the comparison between the data and the results of VMI-1 and VMI-2 at $\gamma = 25^{\circ}$, where both the VMI results have good agreement with the data. The large value of VMI parameter b and small values of C and $\mathcal{I}_0$ indicate comparatively less rigidity against the vibrational degrees of freedom in ^{144}Dy. For such larger values of b, the implementation of VMI in PRM leads to

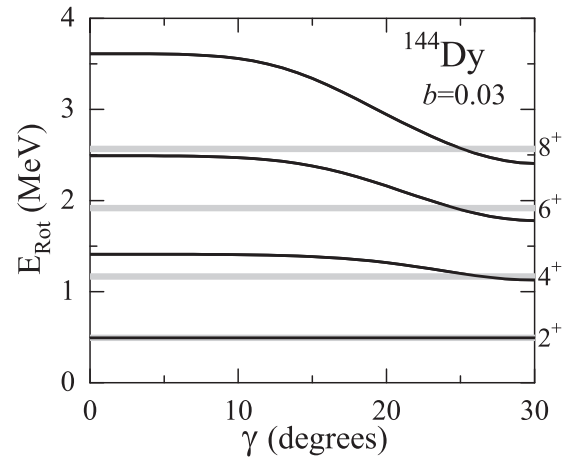

FIG. 5. Rotational spectrum of ^{144}Dy with the parameter b dependent VMI-1 as a function of γ. Grey lines correspond to the experimental spectrum [37]. The black lines represent results from our calculations.

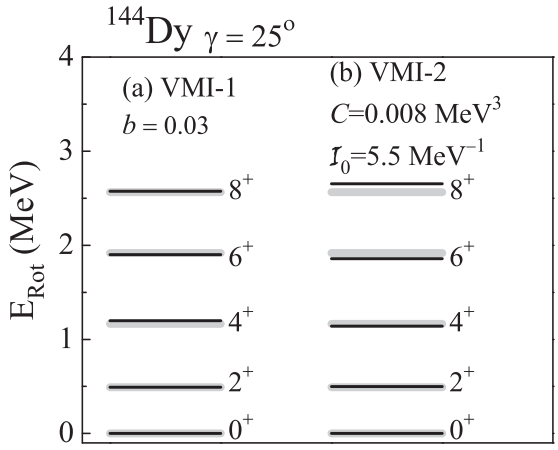

FIG. 6. Rotational spectrum of ^{144}Dy with (a) the parameter b dependent VMI-1 and (b) parameters C and $\mathcal{I}_0$ dependent VMI-2 at $\gamma = 25^\circ$ obtained through best fitting of data. Grey lines correspond to the experimental spectrum and are used in the fit [37]. The black lines represent results from our calculations.

spurious displacement of high angular momentum states, and MPRM does not suffer this drawback [22].

For ^{147}Tm, the single-particle and quasiparticle energies entering the MPRM calculations are shown in Figs. 7(a) and 7(b) as a function of β_2 at $\gamma = 25^\circ$, where the Esbensen-Davids set of parameters [42] is used for the mean field calculations. In Figs. 7(c) and 7(d), the single-particle and quasiparticle energies are presented as a function of γ at $\beta_2 = 0.21$. As γ increases, the negative parity levels come closer to each other, whereas there are many crossings of positive parity levels. It is quite clear that the negative parity state of ^{147}Tm is predominantly originating from the $h_{11/2}$ orbital and hence we include all those levels in our basis. For the positive parity, we include the single-particle levels originating from the $g_{7/2}$, $d_{5/2}$, $s_{1/2}$, and $d_{3/2}$ orbitals in our basis. From the quasiparticle energy diagram, we see that at moderate deformations both the negative and positive parity levels have similar energies. Consequently, the difference between the lowest positive and negative parity band heads will be very small. The lowest positive parity state is observed to be only 68 keV above the ground state, which has negative parity.

We show the negative parity angular momentum states of ^{147}Tm as a function of γ in Fig. 8. The ground band is shown in Fig. 8(a) and its signature partner in Fig. 8(b). It has to be noted that the MPRM results are less sensitive to γ, since these calculations utilize the rotor spectrum where the information of γ is already built in. From this plot, it is clear that the nucleus is neither purely prolate nor oblate, because, near $\gamma \sim 0$ and $\gamma \sim 60^\circ$, the spectrum is far from the observed data. In most of the rotational spectra involving signature partners, the energy states of the favored band lie lower than the energy states of the unfavored band [43]. In this case the ordering of the states $13/2^-$ and $15/2^-$ is reversed. Our results have the correct ordering for these two states only for $\gamma \gtrsim 30^\circ$, and the ordering of the rest of the energy states is correct for $\gamma \lesssim 35^\circ$. Apart from the fit of the energy states with the data, requiring the

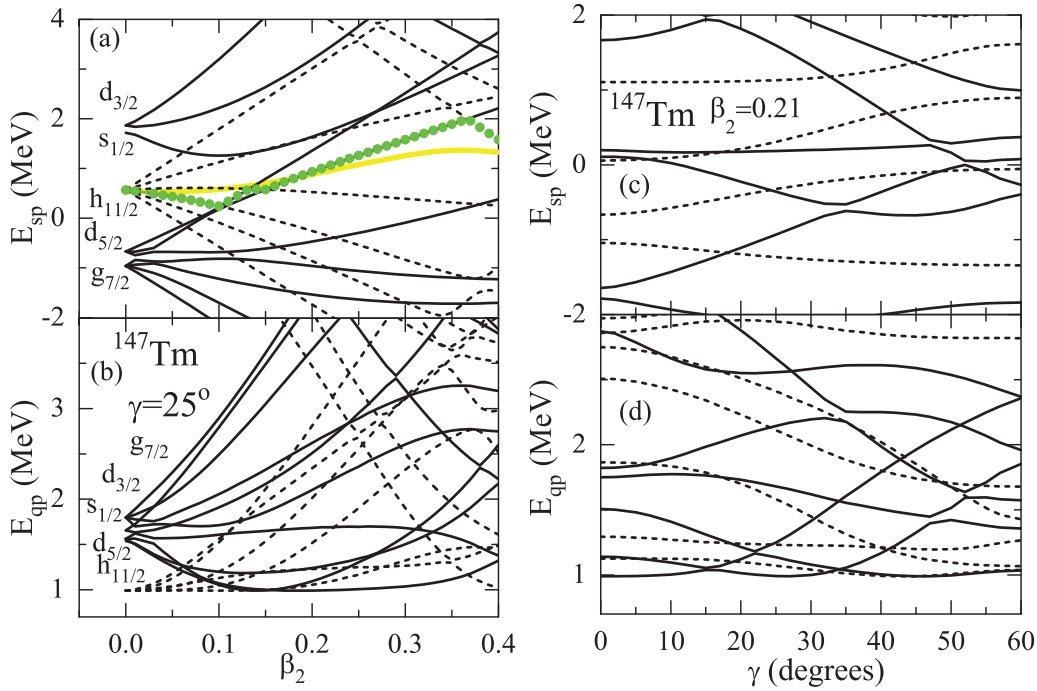

FIG. 7. (a) Single-particle and (b) quasiparticle energies of ^{147}Tm as a function of β_2 at $\gamma = 25^\circ$, and in (c) and (d) as a function of γ at $\beta_2 = 0.21$. These energies are calculated with the Esbensen-Davids set of parameters [42]. γ is adjusted to have the best fit for the rotational spectrum of ^{144}Dy, which is the core for ^{147}Tm. The solid and dashed lines correspond to the positive and negative parity states, respectively. The green dots represent the states of valence particle and the yellow line represents the chemical potential from BCS calculations. At zero deformation the degenerate states are labeled by l_j.

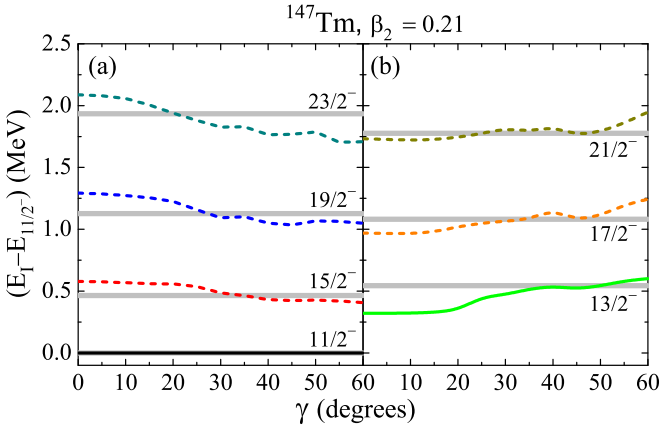

FIG. 8. Negative parity angular momentum states in (a) and their signature partners in (b) as a function of γ at $\beta_2 = 0.21$. The calculation is done with MPRM.

right ordering of the levels suggests that the nucleus exhibits a large triaxiality.

In Fig. 9, the measured negative parity rotational spectrum for ^{147}Tm is compared with our results calculated using PRM and MPRM, where the best fits are achieved at $\gamma = 25^\circ$ and $\beta_2 = 0.21$. The results of MPRM are in better agreement with the observed data. $\gamma = 25^\circ$ is the best fitting γ for the core ^{144}Dy also. For $\gamma = 25^\circ$, the calculated spectrum varies slowly around $\beta_2 \sim 0.2$. With the quadrupole deformation $\beta_2 = 0.21$, we could successfully reproduce the energy difference between two band heads $11/2^-$ and $13/2^-$ of the signature partner bands. This β_2 is consistent with the prediction of the RMF+BCS calculations [40]. These inferences about the deformations are validated further with the aid of the decay data, in the forthcoming text.

We present the half-life of proton emission from the negative parity state of ^{147}Tm in Fig. 10 along with the experimental data. The half-life of proton emission from the $11/2^-$ state has the best agreement with the observed half-life. The calculated half-lives corresponding to the other

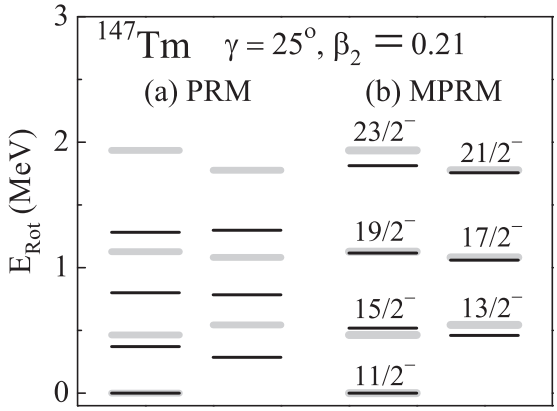

FIG. 9. The negative parity ground state spectrum of ^{147}Tm with its signature partner at $\gamma = 25^\circ$. Grey lines correspond to the experimental spectrum [44]. The black lines represent results of our calculations with MPRM.

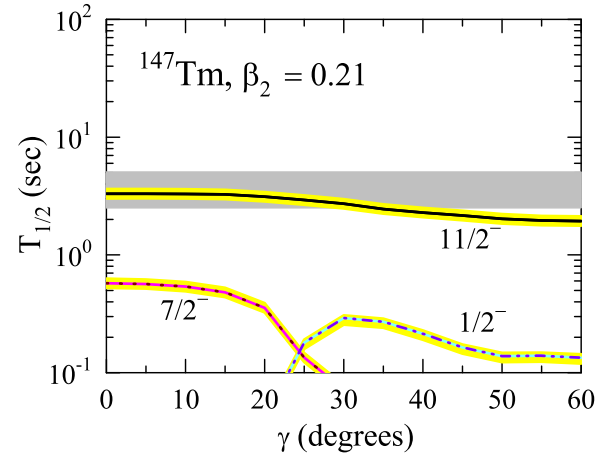

FIG. 10. Half-life of proton emission from the ground state of ^{147}Tm as a function of γ at $\beta_2 = 0.21$. The shaded area in grey corresponds to the experimental values including the errors [45]. The yellow area represents the possible error in the calculated half-life due to the uncertainty in the experimental value of Q_p [45] used as an input in our calculations. Calculated data from other angular momentum states except $1/2^-$ and $7/2^-$ are out of the chosen scale.

lower angular momentum states are out of the chosen scale except for the $1/2^-$ and $7/2^-$ states, which are though energetically not favored. The calculated half-life of the $11/2^-$ state is not very sensitive to γ, but we iterate that in MPRM the major role of the γ deformation is already taken into account through the rotor spectrum. With the ground state of ^{147}Tm clearly established as the $11/2^-$ state, we proceed to analyze the positive parity isomeric state.

In Fig. 11, we present the positive parity states of ^{147}Tm as a function of γ and β_2. From this spectrum, we clearly see that the $5/2^+$ state is the lowest energy state undisputedly at low γ and moderate β_2. Only for $\gamma \gtrsim 30^\circ$ does the $7/2^+$ come closer to the $5/2^+$ state. The $1/2^+$ and $3/2^+$ states are not energetically favored at lower γ and they are competitive to the lowest energy state only when $\gamma \sim 40^\circ$. After $\gamma \sim 40^\circ$ the $3/2^+$ state becomes lowest. However, such a high γ can be ruled out because it cannot explain the spectrum of ^{147}Tm as seen in Fig. 8. In Figs. 11(a) and 11(b), the change in energies

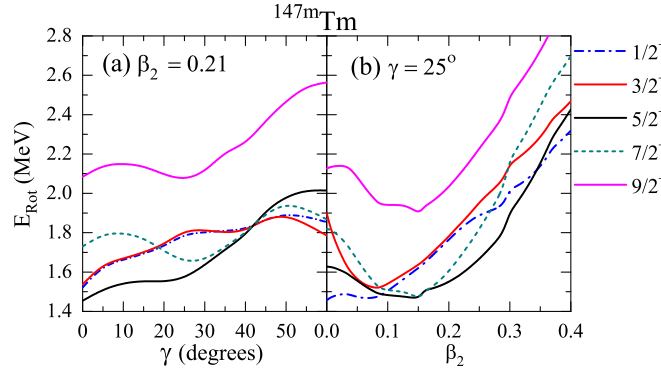

FIG. 11. The calculated energies for positive parity states in ^{147}Tm as a function of (a) γ at $\beta_2 = 0.21$ and (b) β_2 at $\gamma = 25^\circ$.

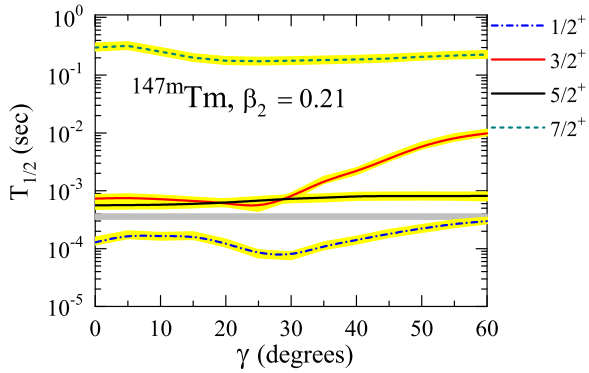

FIG. 12. Similar to Fig. 10 but for proton emission from the positive parity isomeric state of ^{147}Tm.

of $5/2^+$ and $9/2^+$ states follow the same pattern. At $\beta_2 = 0$, the energy difference between $5/2^+$ and $9/2^+$ states equals the E_2^+ (493 keV) of the rotor ^{144}Dy. This shows that $9/2^+$ is built on the $5/2^+$ state. The energy difference between $5/2^+$ and $9/2^+$ states is 500 keV at $\gamma \sim 25^\circ$, $\beta_2 \sim 0.21$ (586 keV at $\gamma \sim 15^\circ$, $\beta_2 \sim 0.21$), which equals the measured energy difference in the $3/2^+$ and $5/2^+$ states in Ref. [25]. Thus from our calculations we observe that $5/2^+$ and $9/2^+$ states are members of the same band and the gamma transition of energy 587 keV measured in Ref. [25] is between $9/2^+$ and $5/2^+$ states. We proceed to validate these arguments by making use of the data of the proton emission from the isomeric state.

The half-life of proton emission from the positive parity isomeric state is shown in Fig. 12. The half-life corresponding to the $5/2^+$ state is near the observed half-life and hence can be confirmed as the proton emitting state. The half-life of $3/2^+$ state also lies near the data for lower γ, but this state is not energetically favored, as seen in Fig. 11. A similar argument is applicable for the $1/2^+$ state also. The half-life of $7/2^+$ state is far from the data by several orders of magnitude. From Fig. 11, up to $\gamma \sim 40^\circ$, the lowest energy state is $5/2^+$, so this state could be the proton emitting state. In Refs. [24,25], the half-lives for ground and isomeric states calculated with the WKB approximation have suggested angular momenta $l = 5$ and $l = 2$, respectively for the ground and isomeric proton emitting states of ^{147}Tm. Based on this, the $h_{11/2}$ and $d_{3/2}$ orbitals were proposed for proton emission from the ground and isomeric states, respectively. Our results suggest that the proton emitting $(5/2^+)$ state is dominated by the $d_{5/2}$ orbital (which also has an angular momentum $l = 2$) and has a significant contribution from the $g_{7/2}$ orbital also.

IV. SUMMARY

With a microscopic approach for rotation-particle coupling, we have analyzed the spectra of proton emitting nuclei ^{141}Ho, ^{145}Tm, and ^{147}Tm. A simple variable moment of inertia (VMI) model suggests clear evidence of γ deformation in their corresponding cores (even-even nuclei). We have demonstrated that the newly developed modified particle-rotor model (MPRM) could unambiguously explain the rotational spectra of the considered proton emitters and yield better agreement with the data when compared to the conventional particle-rotor model (PRM). In the case of ^{147}Tm, the MPRM also reproduces the energy difference between two band heads of the same configuration. The wave functions from MPRM are utilized to calculate the proton emission half-lives, which are not very different from those obtained with PRM as reported in Refs. [16] and [17] for the nuclei ^{141}Ho and ^{145}Tm, respectively. The proton emitting ground state in ^{147}Tm is confirmed as $11/2^-$ and the isomeric state emitting a proton is predicted to be $5/2^+$ from our calculations, which has predominant contributions from the $d_{5/2}$ and $g_{7/2}$ orbitals.

ACKNOWLEDGMENT

This work is supported by the Council of Scientific and Industrial Research, Government of India, via Project No. 03(1338)/15/EMR-II.

[1] M. Thoennessen and B. Sherrill, Nature (London) **473**, 25 (2011).
[2] S. Hofmann, W. Reisdorf, G. Münzenberg, F. P. Heßberger, J. R. H. Schneider, and P. Armbruster, Z. Phys. A **305**, 111 (1982).
[3] O. Klepper, T. Batsch, S. Hofmann, R. Kirchner, W. Kurcewicz, W. Reisdorf, E. Roeckl, D. Schardt, and G. Nyman, Z. Phys. A **305**, 125 (1982).
[4] A. A. Sonzogni, Nucl. Data Sheets **95**, 1 (2002).
[5] D. S. Delion, R. J. Liotta, and R. Wyss, Phys. Rep. **424**, 113 (2006).
[6] C. N. Davids, P. J. Woods, J. C. Batchelder, C. R. Bingham, D. J. Blumenthal, L. T. Brown, B. C. Busse, L. F. Conticchio, T. Davinson, S. J. Freeman *et al.*, Phys. Rev. C **55**, 2255 (1997).
[7] J. C. Batchelder, C. R. Bingham, K. Rykaczewski, K. S. Toth, T. Davinson, J. A. McKenzie, P. J. Woods, T. N. Ginter, C. J. Gross, J. W. McConnell *et al.*, Phys. Rev. C **57**, R1042 (1998).
[8] S. Åberg, P. B. Semmes, and W. Nazarewicz, Phys. Rev. C **56**, 1762 (1997).
[9] E. Maglione, L. S. Ferreira, and R. J. Liotta, Phys. Rev. Lett. **81**, 538 (1998).
[10] E. Maglione, L. S. Ferreira, and R. J. Liotta, Phys. Rev. C **59**, R589 (1999).
[11] L. S. Ferreira and E. Maglione, Phys. Rev. Lett. **86**, 1721 (2001).
[12] G. Fiorin, E. Maglione, and L. S. Ferreira, Phys. Rev. C **67**, 054302 (2003).
[13] M. C. Lopes, E. Maglione, and L. S. Ferreira, Phys. Lett. B **673**, 15 (2009).
[14] M. Patial, P. Arumugam, A. K. Jain, E. Maglione, and L. S. Ferreira, Phys. Lett. B **718**, 979 (2013).
[15] M. Patial, P. Arumugam, A. K. Jain, E. Maglione, and L. S. Ferreira, Phys. Rev. C **88**, 054302 (2013).
[16] P. Arumugam, L. S. Ferreira, and E. Maglione, Phys. Lett. B **680**, 443 (2009).

[17] P. Arumugam, L. S. Ferreira, and E. Maglione, Phys. Rev. C **78**, 041305 (2008).
[18] P. Arumugam, E. Maglione, and L. S. Ferreira, Phys. Rev. C **76**, 044311 (2007).
[19] M. G. Procter, D. M. Cullen, M. J. Taylor, G. A. Alharshan, L. S. Ferreira, E. Maglione, K. Auranen, T. Grahn, P. T. Greenlees, U. Jakobsson *et al.*, Phys. Lett. B **725**, 79 (2013).
[20] M. Patial, Ph.D. thesis, Indian Institute of Technology, Roorkee, 2013 (unpublished).
[21] C. N. Davids and H. Esbensen, Phys. Rev. C **69**, 034314 (2004).
[22] S. Modi, M. Patial, P. Arumugam, E. Maglione, and L. S. Ferreira, Phys. Rev. C **95**, 024326 (2017).
[23] S. Modi, M. Patial, P. Arumugam, E. Maglione, and L. S. Ferreira, Phys. Rev. C **95**, 054323 (2017).
[24] P. J. Sellin, P. J. Woods, T. Davinson, N. J. Davis, K. Livingston, R. D. Page, A. C. Shotter, S. Hofmann, and A. N. James, Phys. Rev. C **47**, 1933 (1993).
[25] D. Seweryniak, C. N. Davids, W. B. Walters, P. J. Woods, I. Ahmad, H. Amro, D. J. Blumenthal, L. T. Brown, M. P. Carpenter, T. Davinson *et al.*, Phys. Rev. C **55**, R2137 (1997).
[26] K. S. Toth, D. C. Sousa, P. A. Wilmarth, J. M. Nitschke, and K. S. Vierinen, Phys. Rev. C **47**, 1804 (1993).
[27] S. Modi, M. Patial, P. Arumugam, E. Maglione, and L. S. Ferreira, Phys. Scr. **92**, 094002 (2017).
[28] A. Bohr and B. R. Mottelson, *Nuclear Structure* (Benjamin, New York, 1969), Vol. I.
[29] W. Greiner and J. A. Maruhn, *Nuclear Models* (Springer-Verlag, Berlin, 1996).
[30] M. A. J. Mariscotti, G. Scharff-Goldhaber, and B. Buck, Phys. Rev. **178**, 1864 (1969).
[31] H. Toki and A. Faessler, Z. Phys. A **276**, 35 (1976).
[32] G. J. Chen, Y. X. Liu, H. C. Song, and H. Cao, Phys. Rev. C **73**, 034304 (2006).
[33] A. S. Davydov and G. F. Filippov, Nucl. Phys. **8**, 237 (1958).
[34] W. Królas, R. Grzywacz, K. P. Rykaczewski, J. C. Batchelder, C. R. Bingham, C. J. Gross, D. Fong, J. H. Hamilton, D. J. Hartley, J. K. Hwang *et al.*, Phys. Rev. C **65**, 031303 (2002).
[35] D. M. Cullen, M. P. Carpenter, C. N. Davids, A. M. Fletcher, S. J. Freeman, R. V. F. Janssens, F. G. Kondev, C. J. Lister, L. K. Pattison, D. Seweryniak *et al.*, Phys. Lett. B **529**, 42 (2002).
[36] D. Seweryniak, P. J. Woods, J. J. Ressler, C. N. Davids, A. Heinz, A. A. Sonzogni, J. Uusitalo, W. B. Walters, J. A. Caggiano, M. P. Carpenter *et al.*, Phys. Rev. Lett. **86**, 1458 (2001).
[37] L. Goettig, W. Gelletly, C. J. Lister, R. Moscrop, B. J. Varley, and R. Wadsworth, Nucl. Phys. A **464**, 159 (1987).
[38] M. Karny, R. K. Grzywacz, J. C. Batchelder, C. R. Bingham, C. J. Gross, K. Hagino, J. H. Hamilton, Z. Janas, W. D. Kulp, J. W. McConnell *et al.*, Phys. Rev. Lett. **90**, 012502 (2003).
[39] P. Möller, J. R. Nix, W. D. Myers, and W. J. Swiatecki, At. Data Nucl. Data Tables **59**, 185 (1995).
[40] J. M. Yao, B. Sun, P. J. Woods, and J. Meng, Phys. Rev. C **77**, 024315 (2008).
[41] P. Möller, R. Bengtsson, B. G. Carlsson, P. Olivius, T. Ichikawa, H. Sagawa, and A. Iwamoto, At. Data Nucl. Data Tables **94**, 758 (2008).
[42] H. Esbensen and C. N. Davids, Phys. Rev. C **63**, 014315 (2000).
[43] S. G. Nilsson and I. Ragnarsson, *Shapes and Shells in Nuclear Structure* (Cambridge University Press, Cambridge, 1995).
[44] N. Nica, Nucl. Data Sheets **110**, 749 (2009).
[45] B. Blank and M. Borge, Prog. Part. Nucl. Phys. **60**, 403 (2008).